ngVLA Antenna Memo # 5

Measurements of the ngVLA W-band Feed Horns

Lisa Locke, Sivasankaran Srikanth
Central Development Laboratory, NRAO

Carla Beaudet
Green Bank Observatory

July 10, 2019

Abstract

Two prototype W-band (70 – 116 GHz) feed horns were evaluated for the Next Generation Very Large Array (ngVLA) by measuring input reflection coefficients at the NRAO Central Development Lab (CDL) and far-field radiation patterns at the Green Bank Observatory's Anechoic Chamber Antenna Range. Both horn designs have corrugations in the axial direction. The first horn, scaled from a design by Lynn Baker at NRC designed for a 55° half-angle subreflector was machined and plated at the CDL. The second horn, supplied by EMSS in South Africa is designed for a 58° half-angle subreflector. Both horns show circularly symmetric radiation beam patterns, good input reflection coefficient, machinable designs, and excellent aperture efficiencies for the ngVLA prototype 18 m offset Gregorian reflector design.

1 Introduction

The Next Generation Very Large Array is a development project of the National Radio Astronomy Observatory comprising the design and construction of a synthesis array of 244 antennas, each 18 m in diameter covering 1.2 – 116 GHz (25 to 0.26 cm). The current ngVLA Reference Design [1] has six frequency bands shown in **Table 1**. The bands B1 and B2 use quad-ridge feed horns, while B3 through B6 use axially corrugated feed horns.

Table 1: ngVLA Reference Design - frequency band designations

Band #	f_{LOW} (GHz)	f_{HIGH} (GHz)
B1	1.2	3.5
B2	3.5	12.3
B3	12.3	20.5
B4	20.0	34.0
B5	30.5	50.5
B6	70.0	116.0

The two prototype horns under evaluation for ngVLA Band 6 at NRAO's Central Development Lab are the following:

> **LB Horn**: This horn designed by Lynn Baker [2], under contract to the National Research Council of Canada (NRC) is a scaled version of the 0.75 to 1.50 GHz feed horn designed for the NRC's DVA-1 antenna, a prototype for the Square Kilometer Array. The horn has eight axial corrugations. It was optimized for maximum gain and minimum spillover temperature on the current ngVLA antenna reference design [1]. This antenna has a 3.5 m subreflector with a 55° half-angle. Two brass horns were machined and gold plated at the CDL.
>
> **EMSS Horn**: This horn, also an axially corrugated horn was supplied by EMSS, South Africa. This company has designed and fabricated horns and cryogenic receivers for the MeerKAT telescope in the Northern Cape province in South Africa and for the Square Kilometer Array. This horn was scaled from the SKA Band 2 horn (950 – 1760 MHz) with a scaling factor of 95/7000 [3] and was machined out of copper. The EMSS study covered aspects of manufacturability and machining tolerances. This horn has three corrugations, where the depths and widths have been optimized for maximum gain and minimum spillover temperature on the SKA 15 m prototype antenna, which has a 4.6 m subreflector and a 58° half angle.

Figure 1 shows drawings and photographs of the two horns.

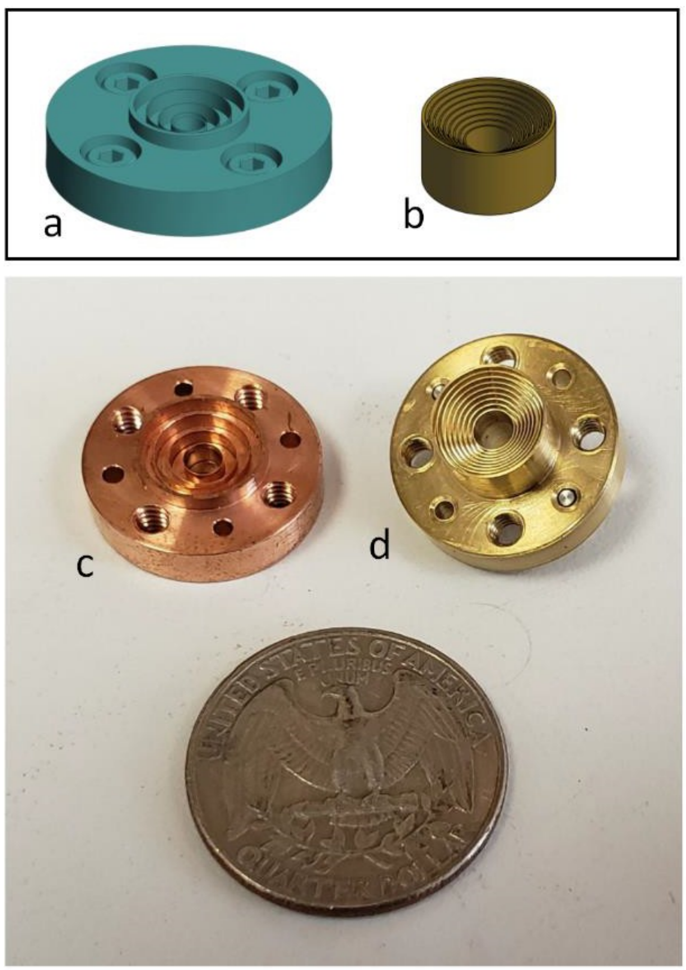

Figure 1: Prototype ngVLA W-band feed horns – drawings and manufactured prototypes. EMSS horn (a,c) and LB horn (b,d). Drawings not to scale with each other. EMSS drawing obtained from [3].

2 MEASUREMENT HARDWARE

In order to measure the input reflection coefficient and far-field radiation patterns of the feed horns, an existing transition was used to interface between the circular waveguide port of the feed horns and the WR-10 rectangular port of the measurement equipment. The transition has a circular diameter of 0.132" and is shown in **Figure 2**.

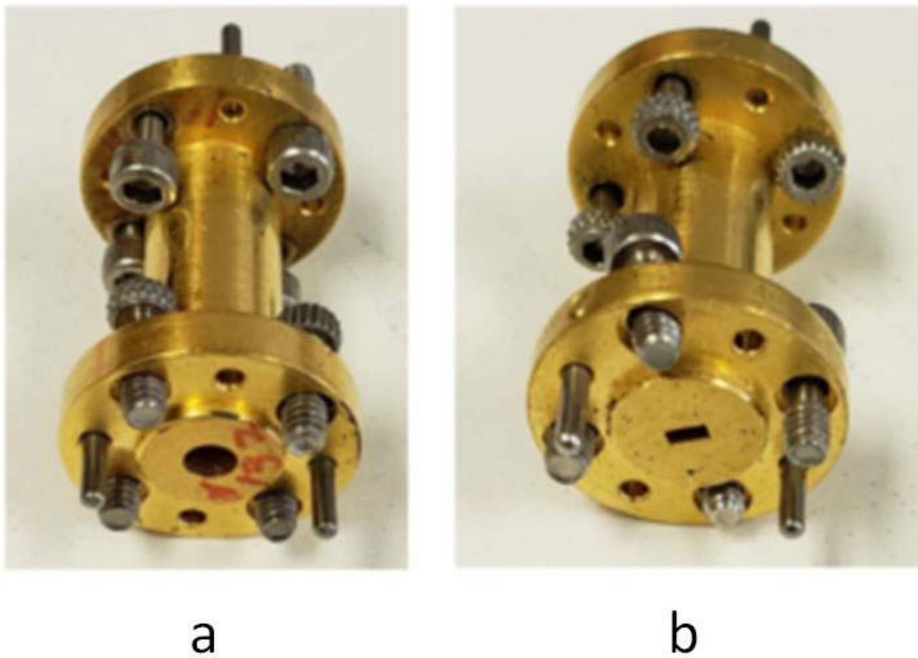

Figure 2: Circular (0.132" Ø) to WR-10 transition, showing both ends. a) circular end b) WR-10 end.

The circular waveguide for the LB feed horn is 0.128" (3.25 mm) in diameter, and the EMSS feed horn is 0.107" (2.73 mm). The larger diameter step for the EMSS horn to the transition affects the input reflection coefficient measurement slightly, which will be discussed within the results section.

3 INPUT REFLECTION COEFFICIENT, $|S_{11}|$

A vector network analyzer with frequency extenders for the 75-115 GHz range was used to measure the input reflection coefficient $|S_{11}|$ of the LB and EMSS horns at the CDL. Two-port TRL calibration was performed at the WR-10 waveguide ports and as a result, the measured reflection coefficient includes the mismatch of the circular to rectangular transition.

The measured reflection coefficient of the EMSS horn is better than 20 dB as shown in **Figure 3** along with the simulated values. The discrepancy of the measured results compared to simulation and the standing waves can be attributed to the mismatch of the waveguide diameters (0.132" to 0.107").

For the LB horn, the simulated and measured results agree well, due to the performance of the horn and the very similar diameters of the horn (0.128") and the transition (0.132"). The average measured values track the simulation well up to 95 GHz. Except for the section between 70.0 GHz at -18.6 dB and 71.9 GHz, the rest of the band stays well below -20 dB. The measured results exhibit a ripple including peaks at 70.8 GHz and 111.8 GHz due to a small reflection in the measurement setup, also seen in the EMSS measured curve.

The LB horn has slightly better performance over the band. If more accuracy is desired for the EMSS measurements a transition will need to be fabricated or procured to better match the EMSS horn.

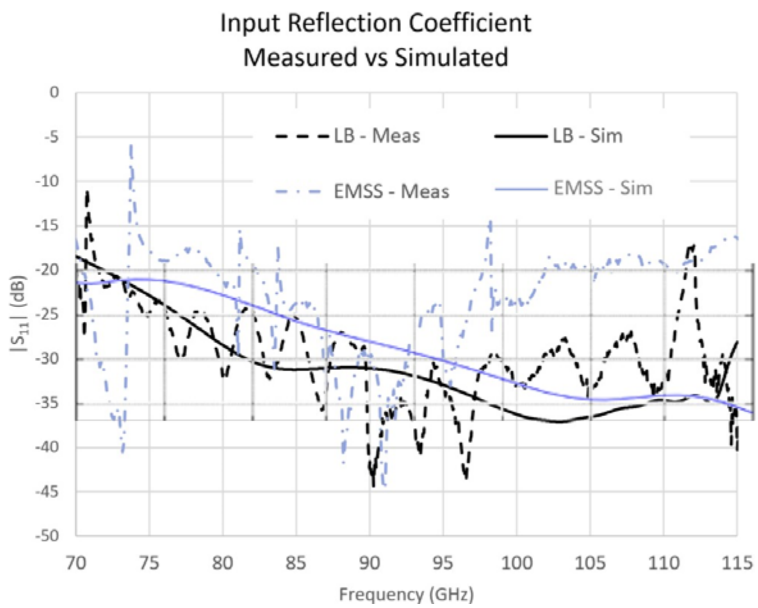

Figure 3: Measured (dashed line) and simulated (solid line) input reflection coefficient of the LB (black) and EMSS (blue) W-band horns. The simulated EMSS data is from [3].

4 Radiation Patterns

4.1 Antenna Measurement Setup

The co-polar and cross-polar radiation patterns were measured in the anechoic chamber antenna range at the Green Bank Observatory on May 2-3, 2019.

Anechoic Chamber

The anechoic chamber provides a controlled environment that minimizes RFI, simulates free-space conditions, and provides a controlled environment compared to outdoor ranges. The large rectangular chamber is capable of measuring far-field patterns of feed horns from 4 GHz to 115 GHz, limited at the lower frequencies by the dimensions of the chamber and at the higher frequencies by the RF equipment [4].

Far-field Setup

The setup outlined in **Figure 4** describes the far-field measurement antenna test range within the anechoic chamber. A transmitting standard gain horn is placed on the stationary tower, at a distance from the antenna under test (AUT) which satisfies the far-field criterion of greater than $\frac{2D^2}{\lambda}$. Here D is the aperture diameter of the AUT and λ is the wavelength at the lowest frequency of measurement. The minimum far-field distance is calculated to be 20 cm, which is easily surpassed with the actual setup shown in **Figure 5**. The AUT is placed on a tower that rotates around its vertical (y) axis, sweeping in azimuth (θ), for each pattern cut.

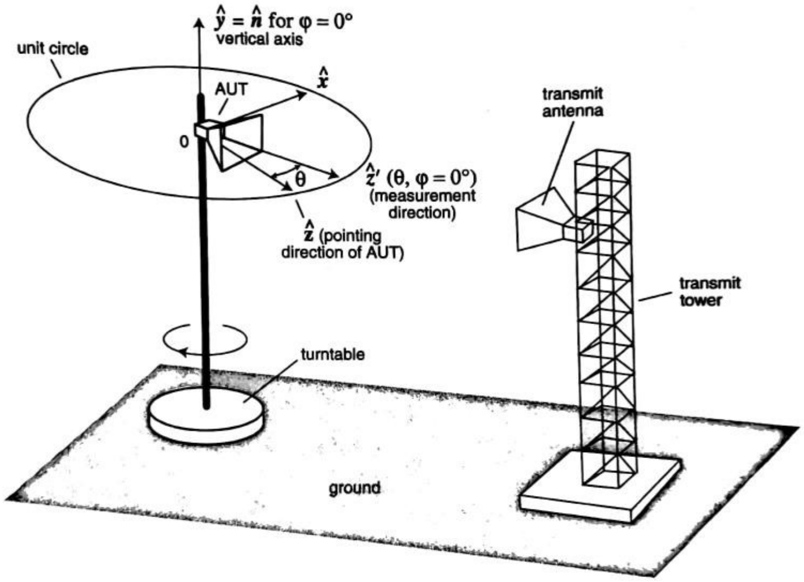

Δ

Figure 4: Far-field antenna test setup for measuring co-polar and cross-polar radiation patterns. The horn under test is placed at "AUT" and aligned in x and z, so that the phase center is directly in line with the tower's axis of rotation. The azimuth, θ angle is measured in the x-z plane with boresight defined at θ = 0. The cut planes are defined by phi, as the angle away from x in the x-y plane. With the AUT as shown, the H-plane is being measured. Image from [5] , p. 46.

4.2 Cut Planes and Frequency Details

Three measured cut planes in phi (ϕ) are defined as follows: H (θ, ϕ = 0°), D (θ, ϕ = 45°), and E (θ, ϕ = 90°) as in **Figure 4**. The sweep in the azimuth (θ) direction is from -175° to +175° in 1° steps. Co-polar patterns in H-, D-, and E-planes and cross-polar patterns in D-plane are measured. The frequency limits of the RF setup of the anechoic chamber at W-band is 75 – 115 GHz and measurements are taken in 2 GHz steps.

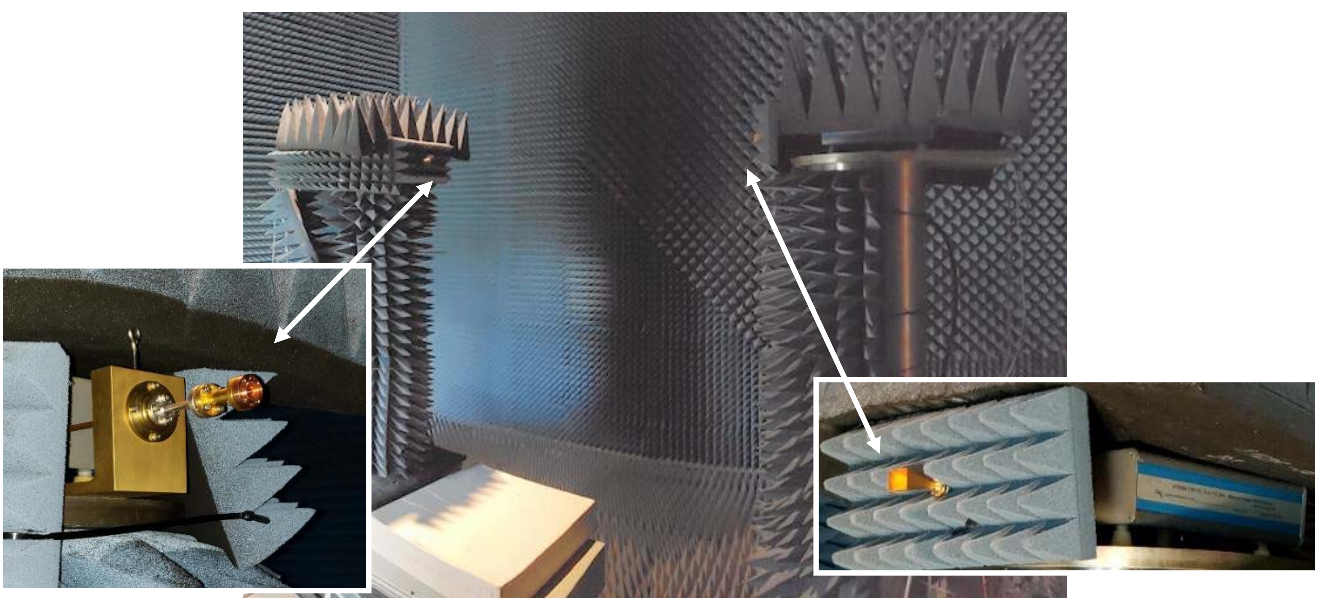

Figure 5: Far-field antenna test setup in the anechoic chamber at Green Bank Observatory, May 2-3, 2019. The stationary tower at right holds the transmitting horn, a pyramidal standard gain horn. The left tower holds the AUT, the tower and base rotate around the phase center of the horn.

4.3 PHASE CENTERS

The AUT is placed with its phase center, computed from simulation, in line with the axis of rotation of the AUT tower. The phase as a function of azimuth is then measured and incremental adjustments are made by moving the AUT in x and z directions as defined in **Figure 4** to achieve the flattest phase response. The final phase centers for 105 GHz for both LB and EMSS horns are noted in **Table 2**.

Table 2: Measured phase centers (x, z) of the LB and EMSS feed horns at 105 GHz

Horn	H-plane (ϕ = 0°)	D-plane (ϕ = 45°)	E-plane (ϕ = 90°)
LB	(0, 0.220”)	(0, 0.220”)	(0, 0.220”)
EMSS	(0, 0.187”)	(0, 0.187”)	(0, 0.187”)

4.4 LB Horn Radiation Patterns

Figures 6 through **11** comprise all the radiation patterns for the LB horn for frequencies 75 – 115 GHz. Principal co-polar and cross-polar cuts, both simulated (solid line) and measured (dotted line), are shown in **Figure 6**. **Figures 7** and **8** superimpose frequency cuts of co-polar normalized gains in the H- and E-planes, respectively. The 3D surface plots show frequency dependence of co-polar normalized gains in the H- (**Figure 9a**) and E- (**Figure 9b**) planes, and cross-polar normalized gains in the D-plane in **Figure 9c**. 3D surface plots of co-polar phase for the H- and E-planes are shown in **Figures 10a** and **10b,** respectively. Co-polar phase cuts for the H- and E-planes are shown in **Figures 11a** and **11b,** respectively. **Figure 11c** displays the co-polar phase at 95 GHz. The radiation patterns measured in all three planes are noisy for frequencies above 110 GHz due to noise in the range's equipment from low signal strength of the sweeper. As a result, calculated efficiencies are lower for both horns above 109 GHz.

Co-polar Results

From the co-polar gain patterns in **Figures 6** to **9b**, the illumination taper values are derived and presented in **Table 3**. Maximum variation in taper values, marked Δ, portray the deviation in beam shape across cut planes for each frequency, and across frequency for each cut plane. The illumination taper at 55^o varies by a maximum of 1.6 dB and 2.1 dB, in the H- and E-planes, respectively. The difference in taper between the principal planes has a maximum value of 1.6 dB (85 GHz). These results show excellent circular symmetry of the beams, especially at 105 GHz.

Cross-polar Results

The cross-polar cuts shown in **Figure 6** and **9c** are referenced to the maximum D co-polar gain. The peaks of the measured values at 75/85/95/105/115 GHz are -28/-28/-27/-24/-20 dB, a very good result. Excluding the noisy 115 GHz cut, all levels are at or below -24 dB.

Phase Results

The co-polar phase information is plotted in **Figures 10** and **11**. The flattest phase response is at 105 GHz because the measurements were carried out with the feed horn positioned with its phase center at 105 GHz at the center of rotation. Within the boresight region, ±55° in azimuth, the maximum/minimum phase variations are ±16°/±15° in the H-plane and ±18°/±7° in the E-plane.

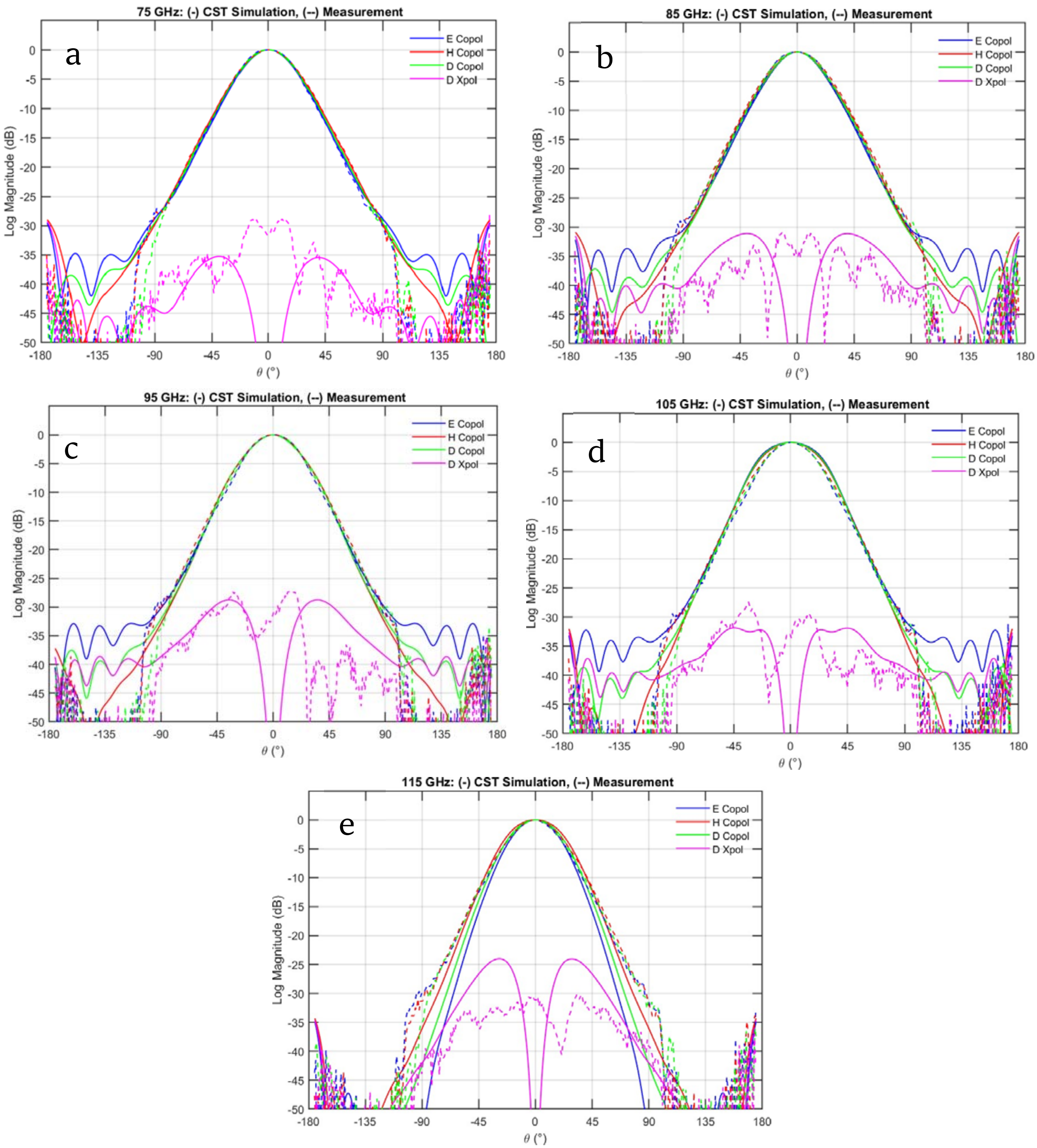

Figure 6: Normalized co- and cross-polar gain for LB horn. Solid line: simulated in CST, dotted line: measured.

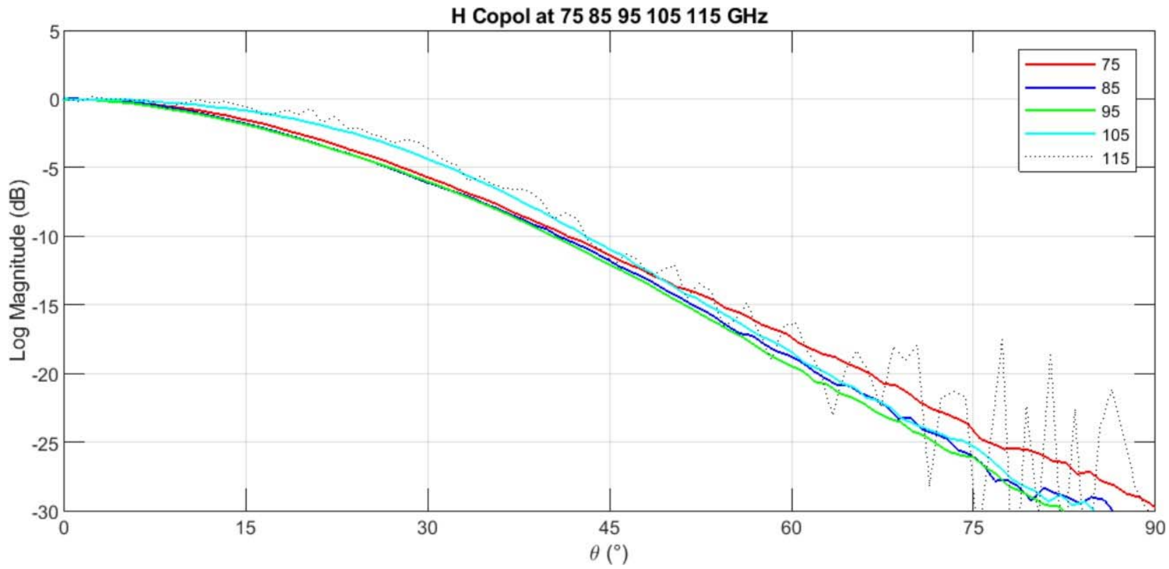

Figure 7: Normalized co-polar gain vs frequency for LB horn, measured. H-plane.

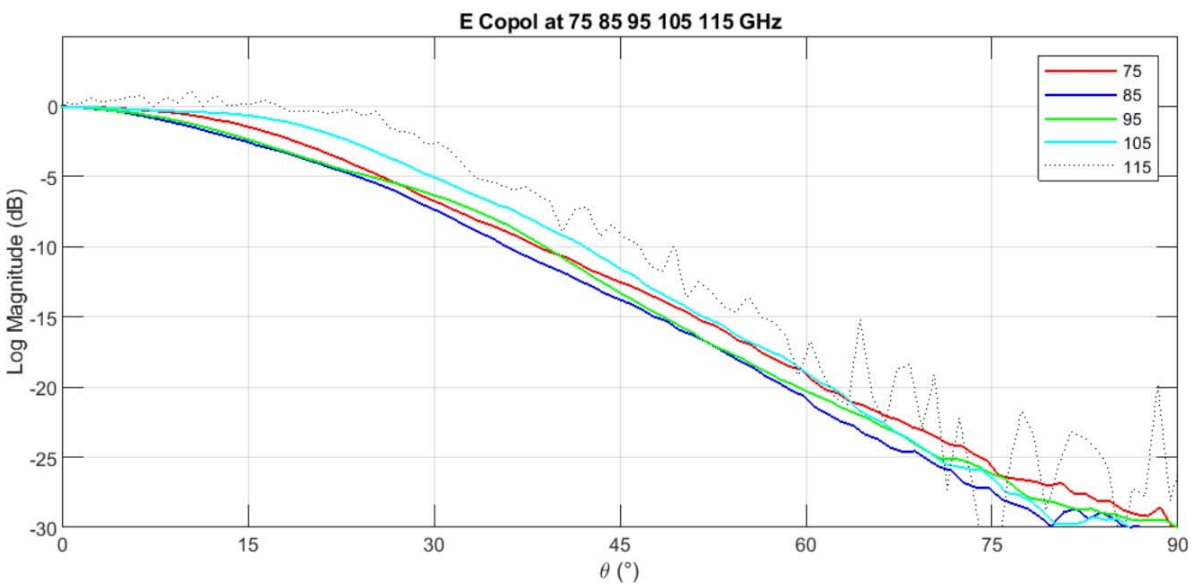

Figure 8: Normalized co-polar gain vs frequency for LB horn, measured. E-plane.

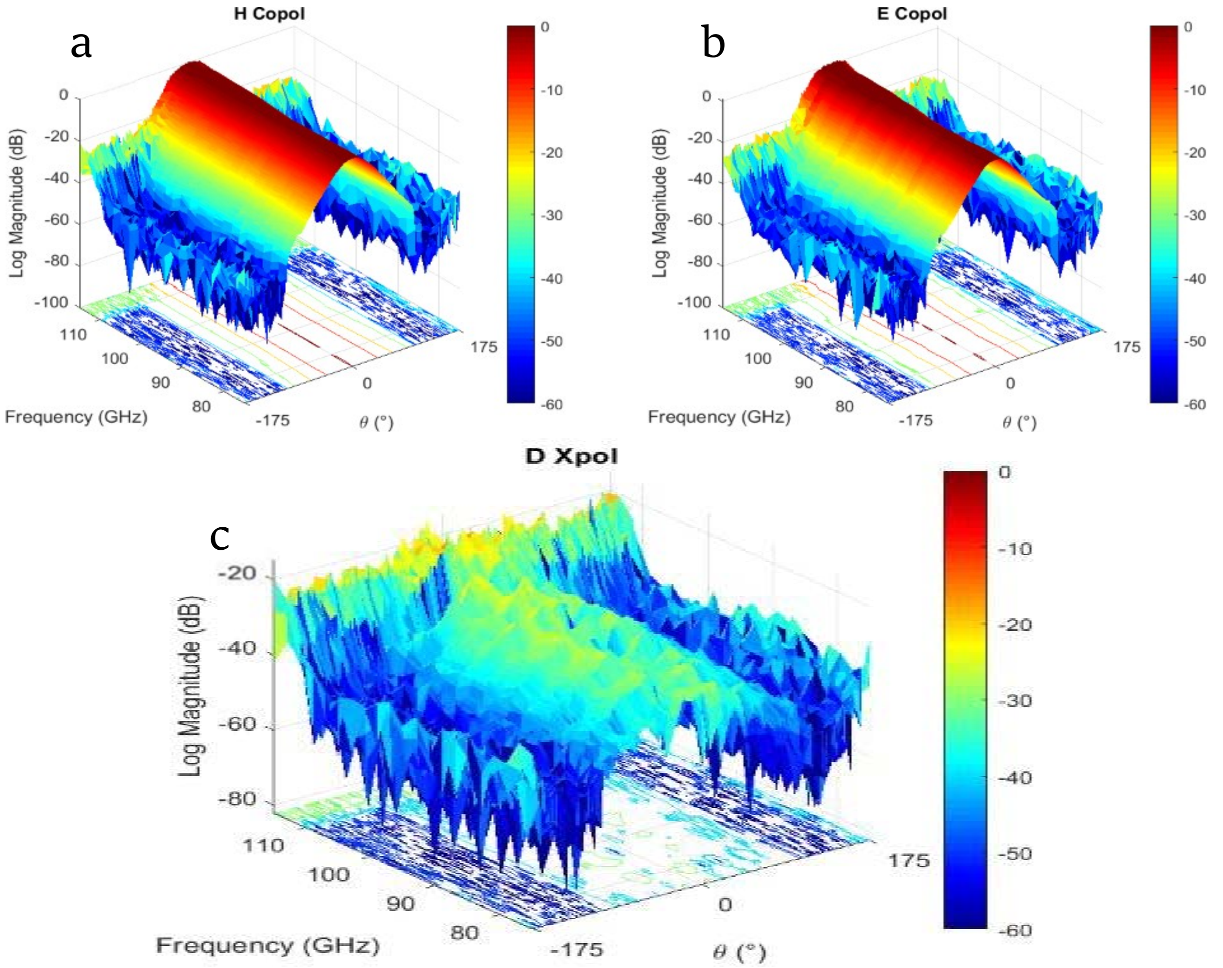

Figure 9: Normalized co-polar gain vs frequency for LB horn, surface plot, measured. a) Co-polar H-plane, b) Co-polar E-plane, c) Cross-polar D plane.

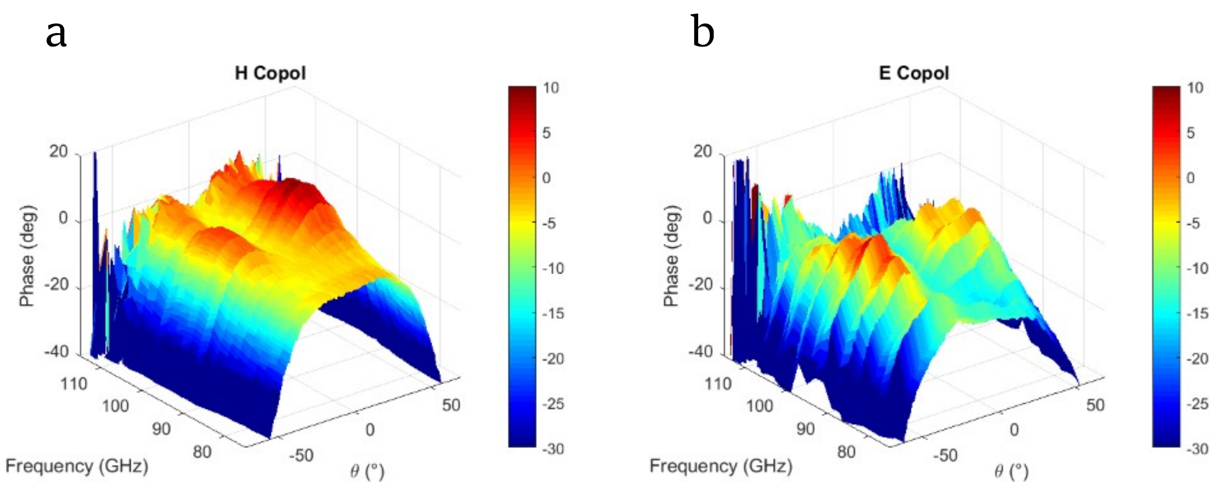

Figure 10: Phase patterns for LB horn, surface plot, measured. a) Co-polar H-plane, b) Co-polar E-plane.

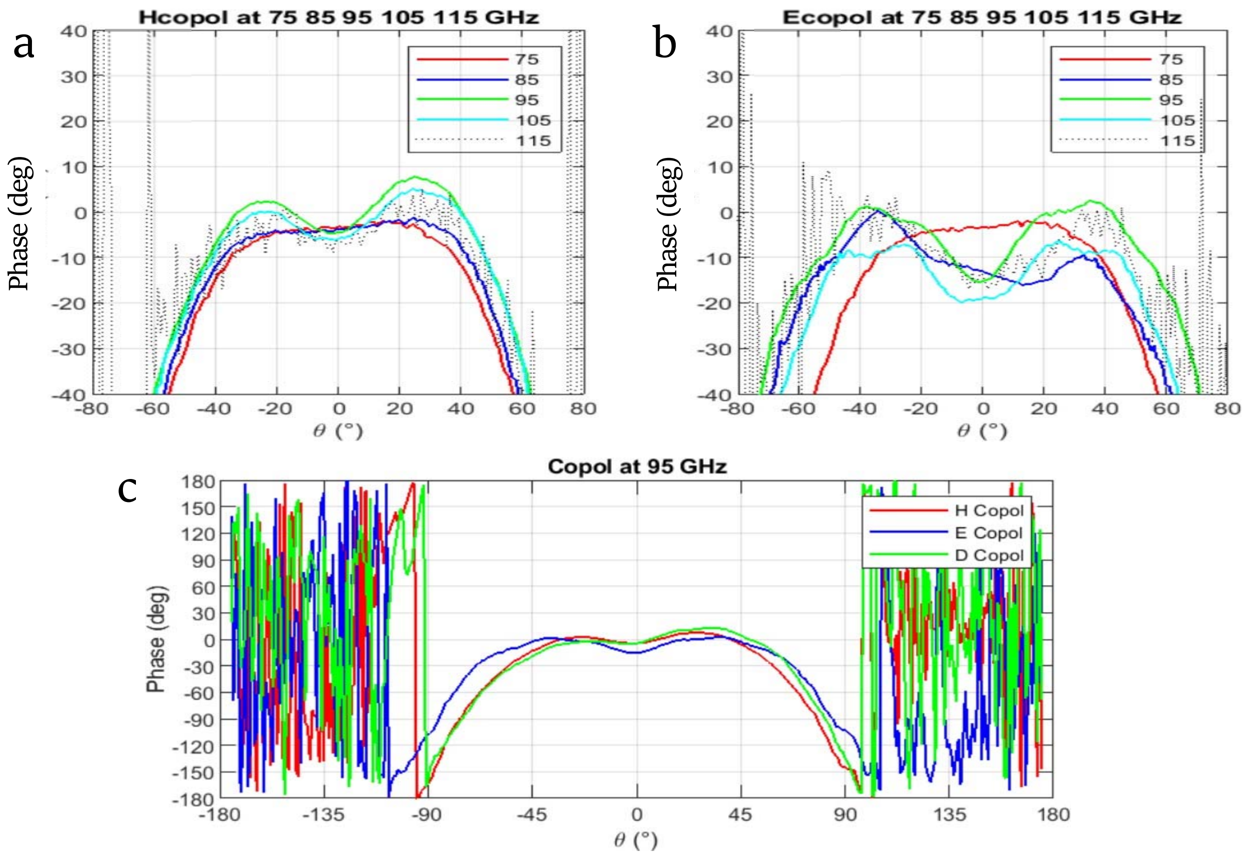

Figure 11: Phase patterns for LB horn, measured. a) Co-polar H-plane vs frequency, b) Co-polar E-plane vs frequency, c) Co-polar, 95 GHz, H, E, and D planes.

Table 3: Co-polar illumination taper values in dB – difference between gain at boresight and gain at θ_M for the 3 cut planes, across the frequency band for LB horn and EMSS horn. Maximum deviation (delta) values across frequencies and cut-planes only compare values from 75 – 105 GHz due to the noisy 115 GHz cuts.

Co-polar illumination taper values (dB) at $\theta = \theta_M$

	LB Horn (θ_M = 55°)				EMSS Horn (θ_M = 58°)			
Frequency	H-plane (ϕ= 0°)	D-plane (ϕ=45°)	E-plane (ϕ=90°)	Δ (dB)	H-plane (ϕ= 0°)	D-plane (ϕ=45°)	E-plane (ϕ=90°)	Δ (dB)
75 GHz	-15.3	-16.0	-16.8	1.5	-14.3	-15.5	-16.1	1.8
85 GHz	-16.7	-17.7	-18.3	1.6	-14.6	-16.0	-17.8	3.2
95 GHz	-16.9	-17.9	-18.0	1.1	-13.1	-14.5	-15.2	2.1
105 GHz	-15.9	-16.1	-16.2	0.3	-12.9	-14.1	-13.3	0.4
115 GHz	-12.2	-14.2	-16.2	N/A	-10.0	-16.2	-9.5	N/A
Δ (dB) 75-105	1.6	1.9	2.1		1.7	1.9	4.5	

4.5 EMSS HORN RADIATION PATTERNS

Figures 12 through **17** comprise all the radiation patterns for the EMSS horn for frequencies 75 – 115 GHz. Principal co-polar and cross-polar cuts, both simulated (solid line) and measured (dotted line) are shown in **Figure 12**. **Figures 13** and **14** superimpose frequency cuts of co-polar normalized gains in the H- and E-planes, respectively. The 3D surface plots show frequency dependence of co-polar normalized gains in the H-(**Figure 15a**) and E-(**Figure 15b**) planes, and cross-polar normalized gains in the D-plane of **Figure 15c**. 3D surface plots of co-polar phase for the H- and E-planes are shown in **Figures 16a** and **16b,** respectively. Co-polar phase cuts for the H- and E-planes are shown in **Figures 17a** and **17b,** respectively**. Figure 17c** displays the co-polar phase at 95 GHz. The radiation patterns measured in all three planes are noisy for frequencies above 110 GHz due to noise in the range's equipment from low signal strength of the sweeper. As a result, calculated efficiencies are lower for both horns above 109 GHz.

Co-polar Results

From the co-polar gain patterns in **Figures 12** to **15b**, the illumination taper values are derived and presented in **Table 3**. Maximum variation in taper values, marked Δ, portray the deviation in beam shape across cut planes for each frequency, and across frequency for each cut plane. The illumination taper at 58° varies by a maximum of 1.7 dB in the H-plane and 4.5 dB in the E-plane in the 75-105 GHz range. The maximum difference in taper between the principal planes is 3.2 dB (85 GHz). These results show good circular symmetry of the beams, especially at 105 GHz. The co-polar beam shapes flatten out as the frequency increases beyond 95 GHz, moving to a slight double-bump at boresight in the H-plane at 105 GHz. This double bump feature increases the aperture efficiency.

Cross-polar Results

The cross-polar cuts shown in **Figures 12** and **15c** are referenced to the maximum D co-polar gain. The peaks of the measured values at 75/85/95/105/115 GHz are -25/-23/-24/-19/-12 dB, a good result. Excluding the noisy 115 GHz cut, all levels are at or below – 19 dB.

Phase Results

The co-polar phase information is plotted in **Figures 16** and **17**. The phase center was adjusted while analyzing the phase at 105 GHz. Within the boresight region, ±58° in azimuth, the maximum/minimum phase variations are ±12°/±10° in the H-plane and ±12°/±8° in the E-plane.

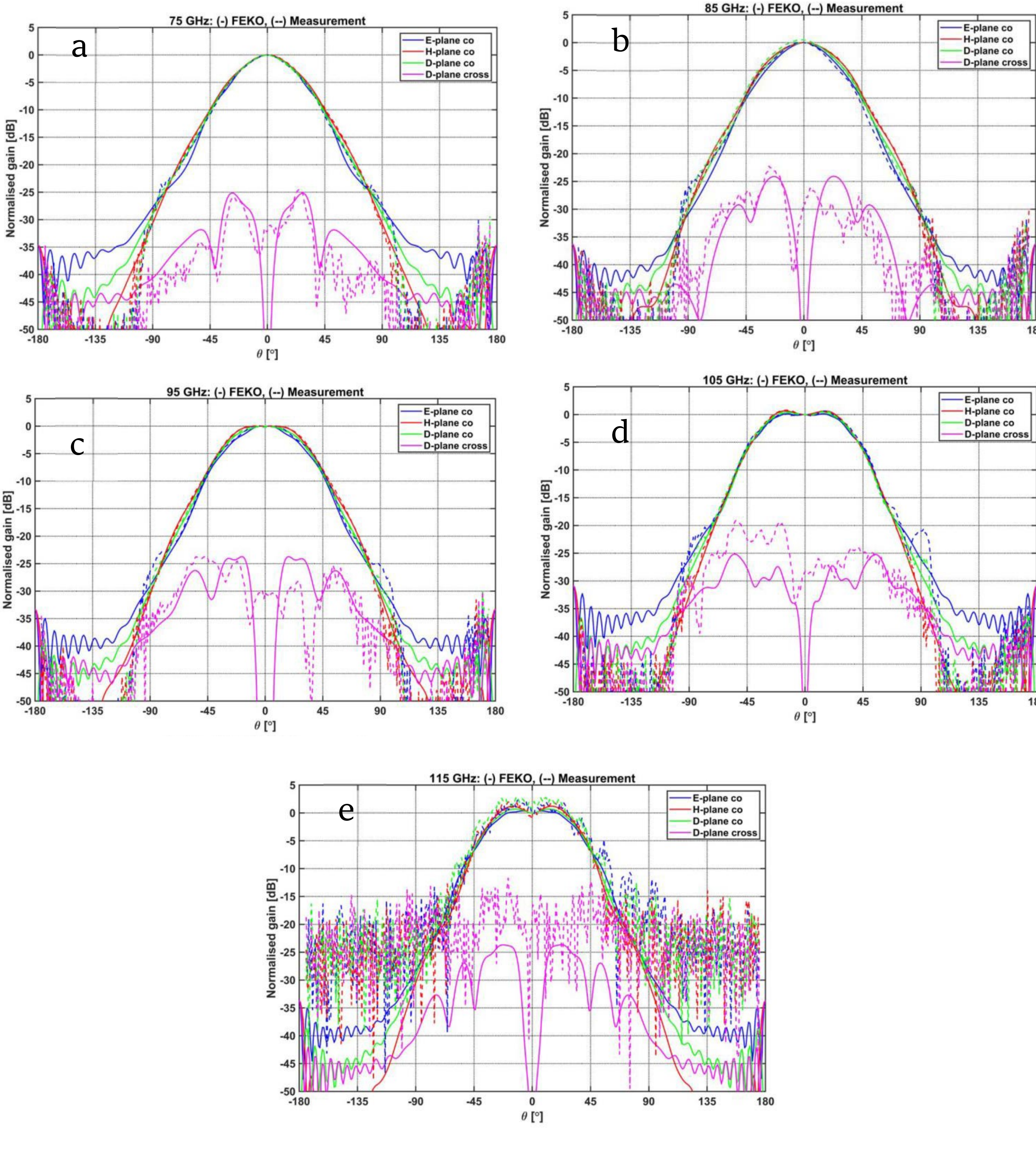

Figure 12: Normalized co- and cross-polar gain for EMSS horn. Solid line: simulated in FEKO [3], dotted line: measured.

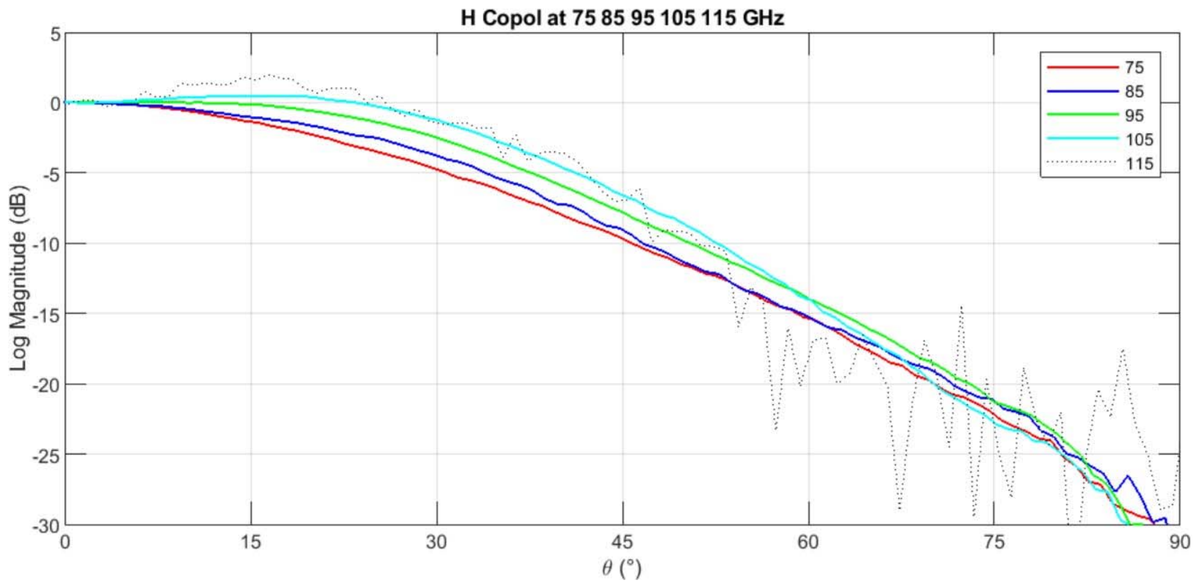

Figure 13: Normalized co-polar gain vs frequency for EMSS horn, measured. H-plane.

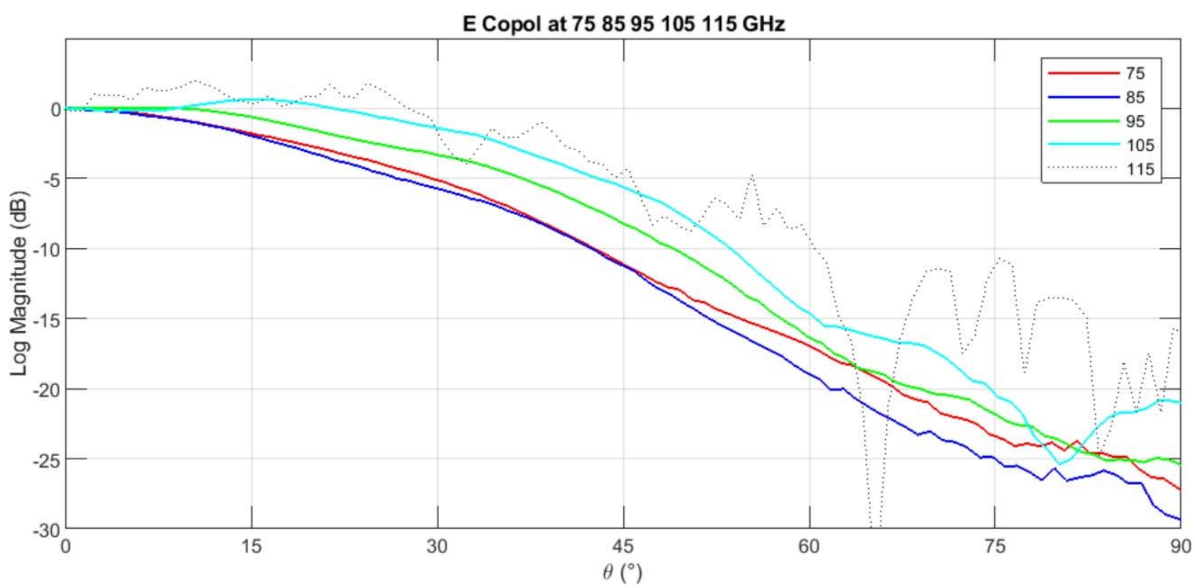

Figure 14: Normalized co-polar gain vs frequency for EMSS horn, measured. E-plane.

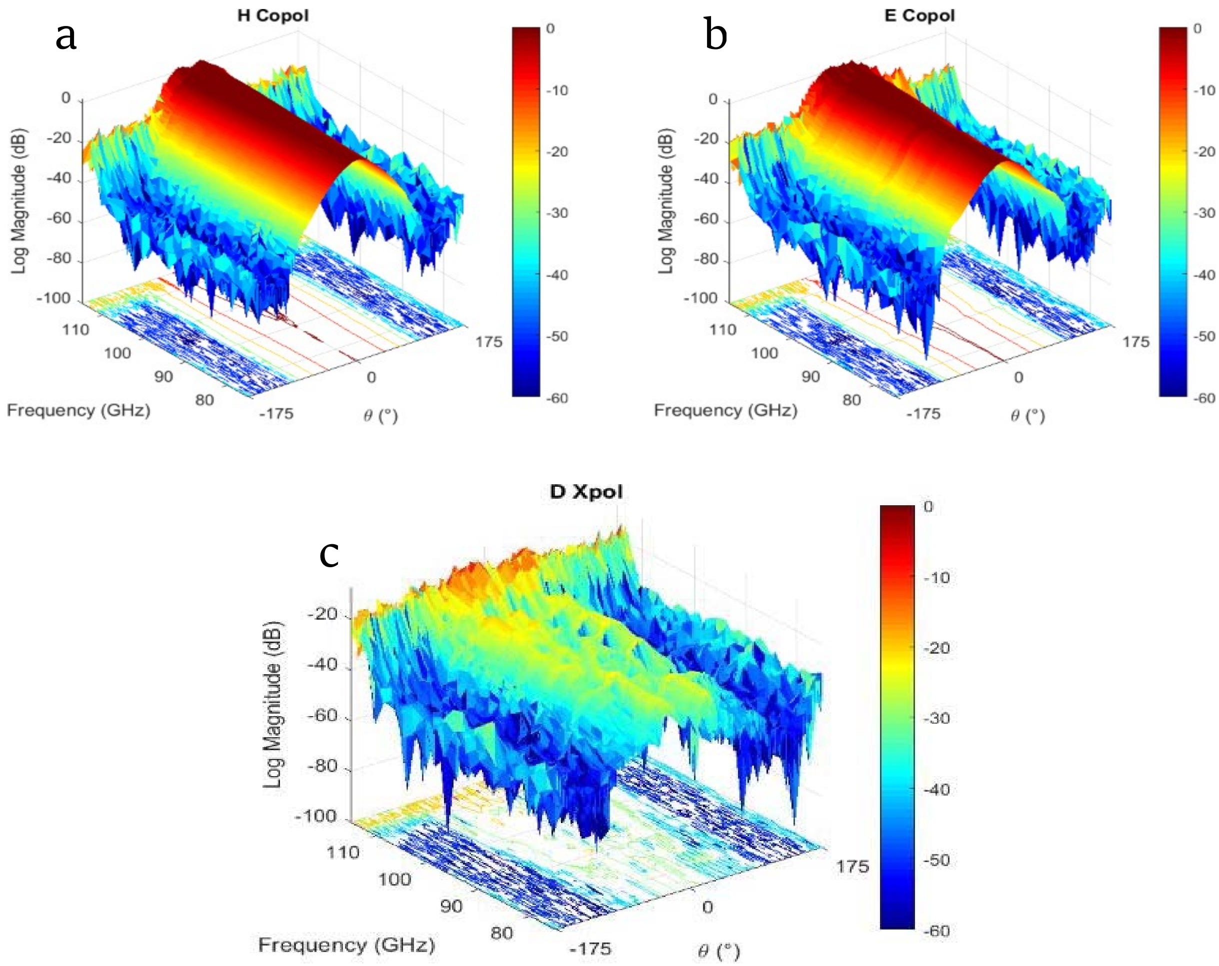

Figure 15: Normalized co-polar gain vs frequency for EMSS horn, surface plot, measured. a) Co-polar H-plane, b) Co-polar E-plane, c) Cross-polar D plane

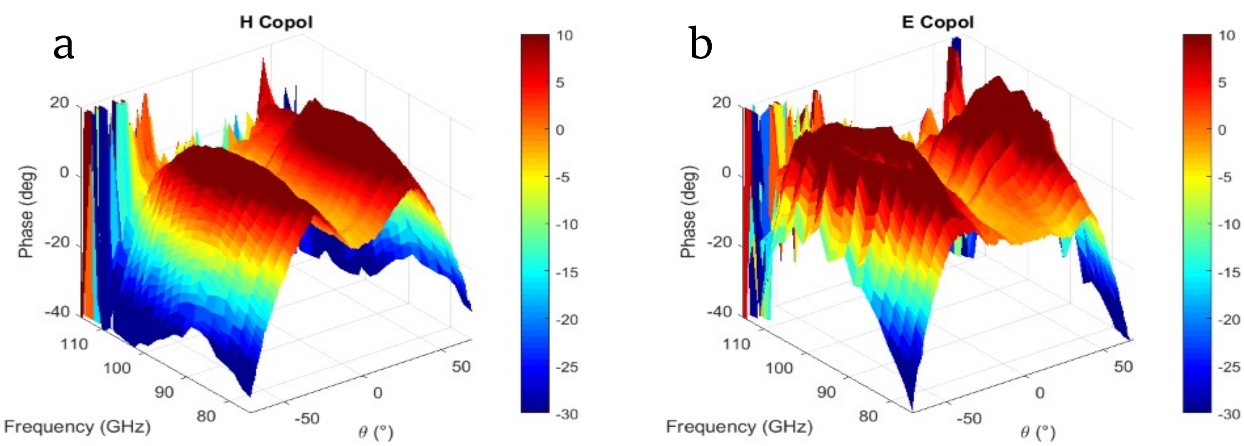

Figure 16: Phase patterns for EMSS horn, surface plot, measured. a) Co-polar H-plane, b) Co-polar E-plane.

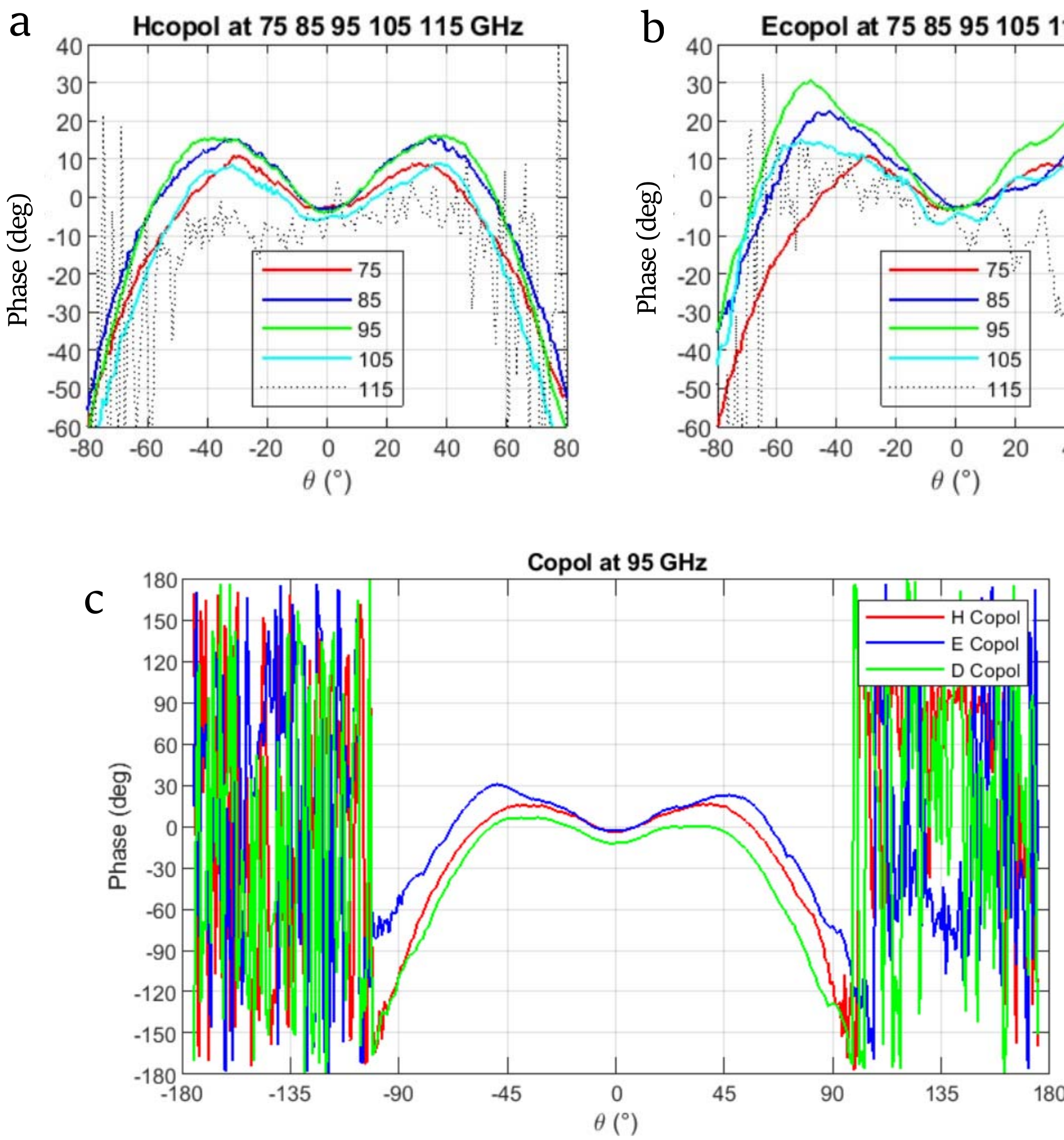

Figure 17: Phase patterns for EMSS horn, measured. a) Co-polar H-plane vs frequency, b) Co-polar E-plane vs frequency, c) Co- polar, 95 GHz, H, E, and D planes.

5 APERTURE EFFICIENCY

The aperture efficiency η_A is the ratio of the maximum effective radiating area, A_e of an antenna to the physical aperture area, A_p. Importing the measured beam patterns into GRASP and using the ngVLA prototype model with shaped surfaces, the aperture efficiency is calculated and plotted in **Figure 18.**

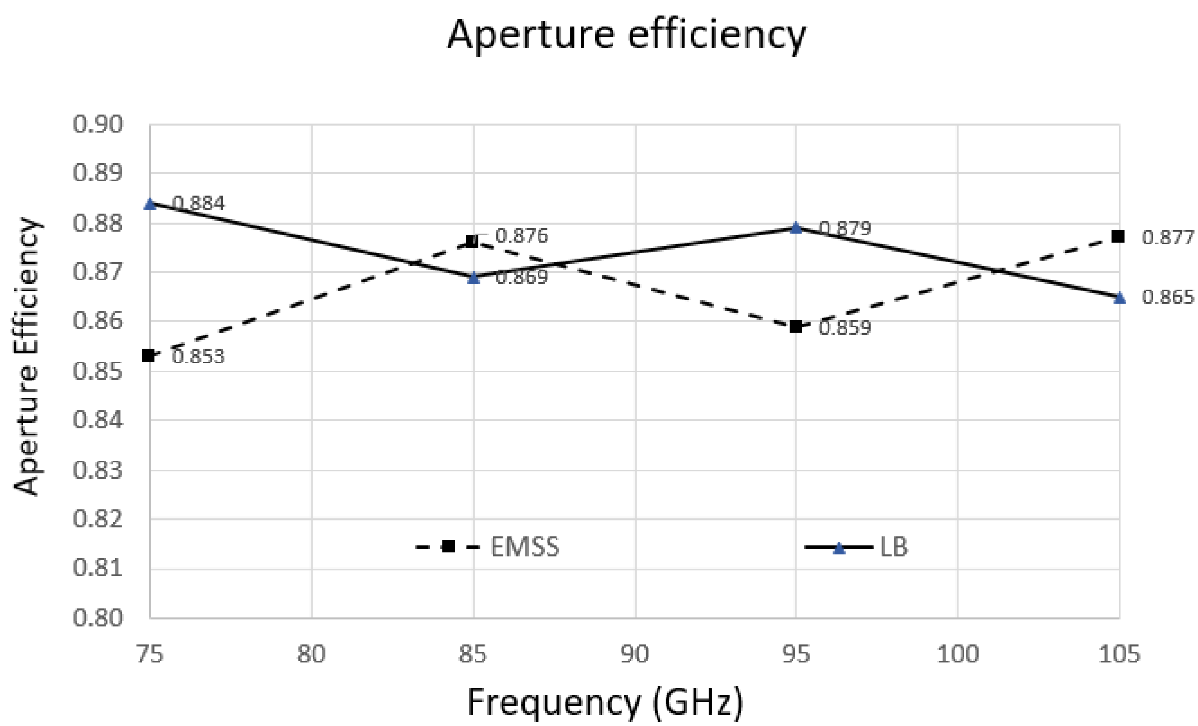

Figure 18: Calculated aperture efficiencies for LB and EMSS horns, from measured radiation pattern using calculations with GRASP and ngVLA prototype model's shaped surfaces.

6 SUMMARY

Two prototype W-band horns for ngVLA's Band 6 are measured over the frequency range of 75 – 115 GHz and evaluated in terms of input reflection coefficient, radiation patterns and aperture efficiency.

Input Reflection Coefficient, $|S_{11}|$

Measured $|S_{11}|$ of the LB horn agrees well with simulations. The simulated $|S_{11}|$ exceeds -20 dB between 73 – 115 GHz and below -25 dB for 77 – 115 GHz. The simulated $|S_{11}|$ of the EMSS horn exceeds -20 dB over the 70 – 115 GHz range and below -25 dB for 84 – 115 GHz. The measurements have good agreement with theory up to 95 GHz. The discrepancy at the higher end of the band is attributed to the mismatch in the circular waveguide diameters of the feed horn and the transition used in the measurement.

Radiation Patterns

The radiation patterns including co-polar and cross-polar gains and phases are excellent for both feed horns. Each have very symmetric co-polar beams in azimuth with a slightly larger H-plane beam. **Figures 6 – 11** show simulated and measured gain and phase patterns for the LB horn. **Figures 12 – 17** show simulated and measured gain and phase patterns for the EMSS horn. Both horns have very symmetric co-polar gains vs frequency, shown in **Figures 6 – 8, 9a** and **9b** and **Figures 12 – 14, 15a** and **15b** for LB and EMSS horns, respectively. This is also represented in **Table 3**, noting the taper value for each horn in each cut-plane for each frequency. Measured illumination tapers at 55° of the LB feed horn vary from 1.6 dB to 2.1 dB over 75 – 105 GHz. The difference in taper between H- and E-planes has a maximum value of 1.6 dB at 85 GHz. The EMSS horn has a larger variation in taper at 58° as a function of frequency, from 1.7 dB to 4.5 dB over 75 – 105 GHz. The difference in taper between H- and E-planes has a maximum value of 3.2 dB at 85 GHz.

Measured D-plane cross-polar gains for 75 – 105 GHz are below -24 dB for the LB horn and below -19 dB for the EMSS horn.

Maximum co-polar phase variations for the LB horn over the boresight region, ±55° in azimuth are ±16°/±18° in the H-/E-planes. For the EMSS horn over the boresight region, ±58° in azimuth the maximum phase variations are ±12°/±12° for the H-/E-planes.

Aperture Efficiency

Incorporating the shaped surfaces of the ngVLA prototype model and the measured beams at four frequencies, 75, 85, 95, and 105 GHz, the LB horn's aperture efficiency values range from 86.5% to 88.4% and for the EMSS horn 85.3% to 87.7% shown in **Figure 18**.

Machinability

Two LB horns were machined and plated at the CDL. Measured $|S_{11}|$ results are very similar. There is good agreement between measured and simulated radiation patterns. These results reinforce the facts that CDL has the capability to machine this feed horn design to the required accuracy and to reproduce it consistently.

The EMSS horn was machined by the designers, and a comprehensive report on the machinability including a tolerance study is available. The EMSS horn results reiterate that this horn also has been fabricated to the required accuracy.

7 REFERENCES

[1] Selina, R. et al, "Next Generation Very Large Array (ngVLA) System Reference Design, version 10," 2019.

[2] L. Baker, "Analysis of ngVLA Design #6 with Ideal and Actual Feed," 2017.

[3] R. Lehmensiek, "Final Report: ngVLA Project," 2019.

[4] G. Anderson, "Millimeter-wave fed measurements using the Green Bank indoor antenna range," 2005.

[5] P.-S. Kildal, Foundations of Antennas - a unified approach, Studentlitteratur, 2000.

[6] K. Pontoppidan, "Electromagnetic properties and optical analysis of the ALMA antennas and front ends," 2008.